J Solid State Electrochem (2004) 8: 693–705
DOI 10.1007/s10008-004-0534-9

ORIGINAL PAPER

Ewa Cholewa · Ian Burgess · Julia Kunze
Jacek Lipkowski

Adsorption of *N*-dodecyl-*N*,*N*-dimethyl-3-ammonio-1-propanesulfonate (DDAPS), a model zwitterionic surfactant, on the Au(111) electrode surface

Received: 2 April 2004 / Accepted: 20 April 2004 / Published online: 3 July 2004

Abstract Electrochemical measurements including cyclic voltammetry, differential capacity, and chronocoulometry have been used to characterize the adsorption behaviors of the zwitterionic surfactant *N*-dodecyl-*N*, *N*-dimethyl-3-ammonio-1-propanesulfonate (DDAPS) on the Au(111) electrode surface. The thermodynamics of the ideally polarized electrode have been employed to determine the Gibbs excess and the Gibbs energy of adsorption. The results show that the adsorption of DDAPS has a multistate character. The first two states are observed at potentials close to zero charge. At low bulk DDAPS concentrations, it corresponds to the formation of a film of nearly flat adsorbed molecules. At higher concentrations it is converted into a hemimicellar state. The second state is formed at negative potentials and charge densities close to 0 μC cm^{-2}. It corresponds to a film of tilted molecules oriented with the hydrocarbon tail towards the metal and the polar head toward the solution.

Keywords Zwitterionic surfactants · Chronocoulometry · *N*-dodecyl-*N*,*N*-dimethyl-3-ammonio-1-propanesulfate · Adsorption at Au(111)

Introduction

There is significant interest in the surface aggregation of ionic [1–12], zwitterionic [5, 13, 14, 15], and neutral surfactants [5, 15, 16]. Recent scanning probe microscopy experiments revealed that surfactants may assemble at a solid-solution interface to form hemicylindrical [1–8, 10, 15, 16], hemispherical and spherical [2, 3, 9, 10, 15], or irregular globular aggregates [16]. These studies have shown that the shape of surface aggregates depends on the interaction of surfactant molecules with the two neighboring phases, and results from the interplay of a number of factors such as: 1) the force required to reduce the contact between water and the hydrocarbon tails; 2) the lateral interaction between the headgroups; 3) the interaction of headgroups with the two phases; 4) packing constraints; 4) entropy of mixing, and; 5) the hydrophilicity and hydrophobicity of the solid surface. The roles of various forces that affect the surface aggregation of surfactants and various packing geometries were discussed recently by Retter et al [17, 18, 19, 20].

We have already shown that at metals, the surface aggregation of anionic surfactant such as sodium dodecyl sulfate (SDS) is controlled by the electrode potential (the charge on the metal) [21, 22]. This observation was confirmed by Petri and Kolb [23]. At small charge densities, SDS molecules aggregate into hemicellar stripe-like surface micelles (hemimicelles). This state is well ordered. The long range order is stabilized by the interaction between the sulfate groups that belong to SDS molecules in adjacent stripes. At large positive charge densities (positive potentials), the hemimicellar aggregates melt to form a condensed film. The surface concentration of SDS molecules doubles upon transition from the hemimicellar to the condensed state. The properties of the condensed film are best explained by a model of an interdigitated film in which half of the sulfate groups are turned toward the metal and half toward the solution [22].

The objective of the present work is to extend our studies of the potential controlled aggregation of surfactants at electrode surfaces to a zwitterionic species. Our goal was to get a better understanding of how the nature of the polar head affects the interaction of the adsorbed surfactant molecule with the metal and the lateral interaction between the polar heads of adjacent

Dedicated to Professor Zbigniew Galus on the occasion of his 70th birthday and in recognition of his many contributions to electrochemistry.

E. Cholewa · I. Burgess · J. Kunze · J. Lipkowski (✉)
Department of Chemistry and Biochemistry,
University of Guelph, Guelph,
Ontario, N1G 2W1, Canada
E-mail: lipkowski@chembio.uoguelph.ca

molecules at the surface. In addition, we were interested to learn how this interaction can be controlled by the potential applied to the metal. Due to their large dipole moments, on the order of 18D [24], the adsorption of zwitterionic surfactants should be greatly influenced by the electrical field at the electrode surface.

N-Dodecyl-*N*,*N*-dimethyl-3-ammonio-1-propanesulfonate (DDAPS) was the zwitterionic surfactant molecule investigated in this project. Its structure is shown in Fig. 1. The aggregation of DDAPS on graphite and mica surfaces has recently been investigated by Ducker et al [12–16]. These studies demonstrated that the geometry of DDAPS aggregates depends on the hydrophilicity of the solid surface. In this paper, we will describe the thermodynamics of DDAPS adsorption at the Au(111) electrode surface, determined with the help of electrochemical techniques. Scanning tunneling microscopy and neutron reflectivity studies of the films formed by this surfactant are in progress and will be reported in a future publication.

Experimental

Commercially-obtained DDAPS (Sigma Ultra, St. Louis, MO, 99.9%) was twice recrystallized from ethanol and thoroughly dried in an Albderhalden drying pistol. Fresh solutions of DDAPS were prepared for all experiments in order to minimize contamination. The electrolyte (sodium fluoride salt) was cleaned in a UV-ozone chamber (Jelight, Irvine CA). All solutions were prepared with Milli-Q ultra-pure water (≥18.2 MΩ).

All glassware was cleaned in hot acid (1:3 HNO_3:H_2SO_4) for approximately 45 min and rinsed thoroughly with Milli-Q ultra-pure water. The single crystal Au(111) working electrode (WE) and gold wire counter electrode (CE), were flame annealed using a Bunsen burner and quenched with Mill-Q ultra-pure water to make sure that the surface was free of contamination. A saturated potassium chloride silver-silver chloride electrode (Ag/AgCl), whose potential was −40 mV versus the saturated electrode calomel (SCE), was used as the reference electrode (RE).

The WE, CE, and RE were connected to a potentiostat (HEKA PG 590). The signals from the WE were in analogue form and transmitted to a data acquisition interface (NI-DAQ 6052E, National Instruments). The DAQ board digitized the analogue signals from the potentiostat and transmitted the digital signals to a PC computer for analyses. Custom software (generously supplied by Prof. Dan Bizzotto, University of British Columbia) was used to collect data for the cyclic voltammetry (CV), differential capacity, and chronocoulometry experiments. CV was performed by applying a potential sweep to the electrode surface at a scan rate of 20 mV s^{-1}. To record differential capacity (DiffC), the signals from the potentiostat were resolved by a lock-in amplifier (EG&G, Model 7265), from which a 25 Hz, 5 mV (rms), AC perturbation was superimposed on a 5 mV s^{-1} DC voltage sweep. In the chronocoulometry experiments the electrode was held at a potential E_{ads}, at which the surfactant molecules formed a film at the electrode surface, for a period of time that was long enough for complete adsorption equilibrium to be established (typically 3 min). Next the potential was stepped to $E_{des} = -1000$ mV, where the film was totally desorbed from the electrode surface and the current transient corresponding to this desorption process was

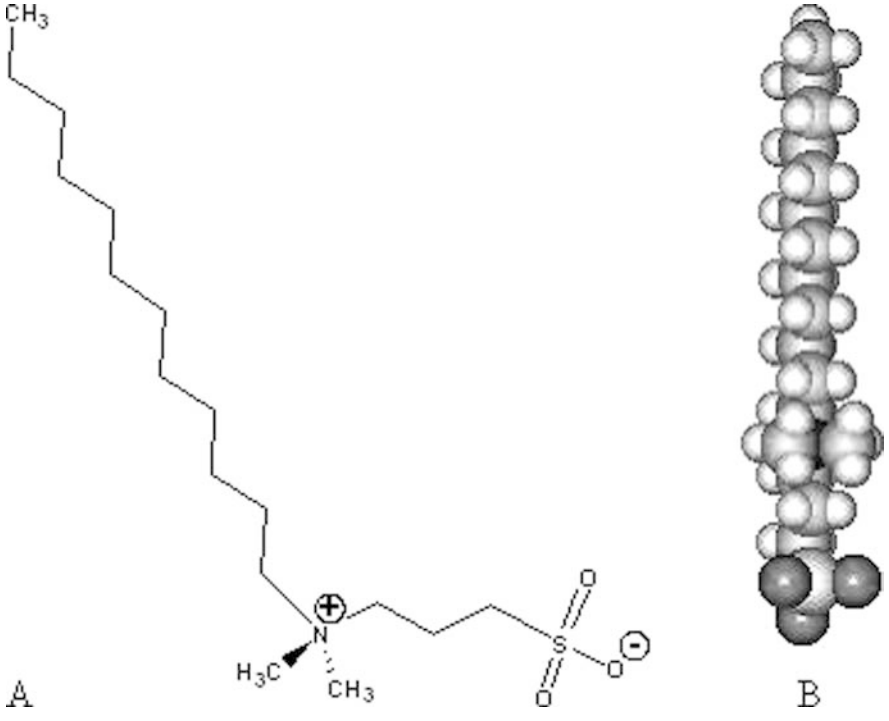

Fig. 1 Models representing the structure of the *N*-dodecyl-*N*, *N*-dimethyl-3-ammino-1-propanesulfonate (DDAPS). **A**: Schematic structure showing the location of positive and negative charges of the zwitterions. **B**: Space filling model showing all of the atoms in the molecule

recorded as a function of time for 200 ms. The current-time curve was integrated to give the relative charge density on the metal surface as a function of the adsorption potential. The potential of zero charge (pzc), determined from an independent experiment to be equal to 310 mV versus Ag/AgCl electrode, was then used to determine the absolute charge density.

The Wilhelmy plate method was used to measure the surface pressure $\pi = (\gamma_o - \gamma_c)$ at the gas/solution interface, where $\gamma_c$is the surface tension at the gas/solution interface in the presence of surfactant molecules andγ_o is the surface tension in the absence of the surfactant molecules. The Wilhelmy plate was a piece of clean filter paper connected to a micro-balance (KSV-Instruments). All experiments were carried out at room temperature (22 ± 2 °C). There was no evidence of DDAPS surfactant precipitation for the experiments conducted at room temperature.

Results and discussion

Critical Micelle Concentration (CMC)

It is known that DDAPS forms micelles in aqueous solutions. In pure water solutions (in the absence of electrolyte ions), the critical micelle concentration (CMC) is 2.2 mM [24]. We wished to confirm this value of the CMC in pure water solutions before progressing to measuring the CMC in electrolyte. The CMC was determined by measuring the surface pressure at the air/solution interface as a function of DDAPS concentration, using the Wilhelmy Plate method. Curve 1 in Fig. 2 plots the surface pressure as a function of the natural logarithm of the DDAPS concentration in a pure aqueous solution (no electrolyte). This measurement was performed with unpurified DDAPS. The surface pressure initially rises but then exhibits a peak before leveling off to reach a quasi plateau. The presence of a maximum in the surface pressure plot indicates that the DDAPS is contaminated with a tensio-active impurity [13]. In an effort to remove this impurity, the DDAPS was twice recrystallised from ethanol. The surface tension measurement was then repeated and is shown as curve 2 in Fig. 2. It is evident that the maximum has been greatly attenuated after the purification and that the surface pressure is systematically lower at all concentrations of DDPS than for curve 1. All remaining experiments were performed using the purified surfactant. The CMC was obtained from the intersection of a polynomial fitted line extrapolated from the measurements obtained below the plateau and the straight fitted line in the plateau on the graph. The CMC value of DDAPS in pure water was found to be 2.2 mM, which is in excellent agreement with the value reported by [24].

The CMC may be different in the presence of the supporting electrolyte and hence it was necessary to determine the CMC in 50 mM NaF solution before performing electrochemical studies of DDAPS adsorption at the Au(111) electrode surface. Curve 3 in Fig. 2 shows the surface pressure plot for the twice recrystallized DDAPS in 50 mM NaF solution. Below the plateau, the two curves are nearly superimposable but the surface pressure levels off at lower surface pressures in the presence of the electrolyte, and a slightly lower CMC is determined (2.1 mM versus 2.2 mM). This result is likely due to a perturbation in the electrostatic interactions between molecules of DDAPS caused by increased

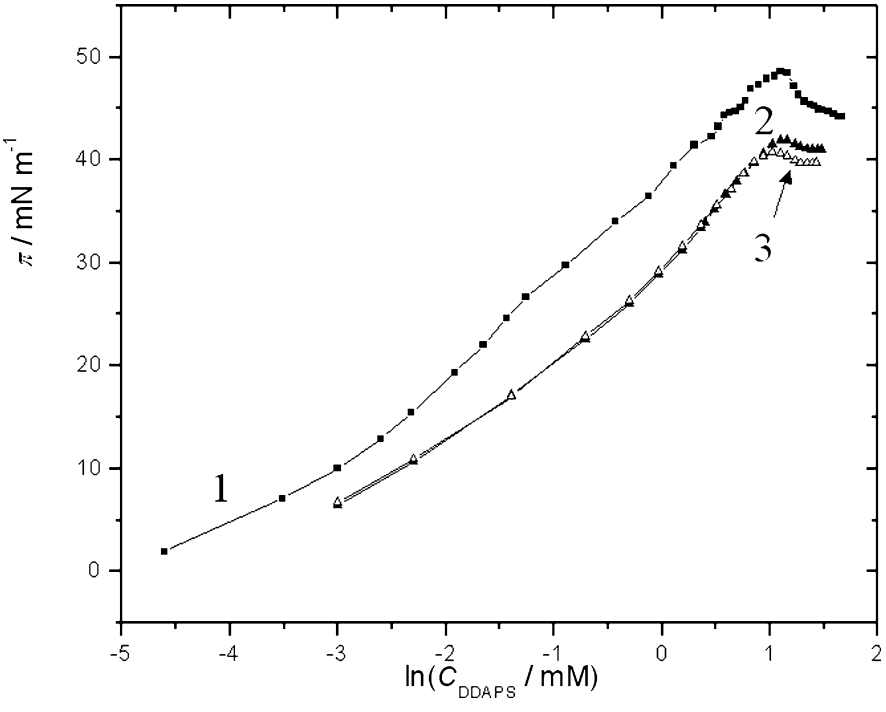

Fig. 2 Plots of the surface pressure at the air-solution interface versus the logarithm of the bulk DDAPS concentration. 1: Unpurified DDAPS solution in pure water. 2: Twice re-crystallized DDAPS solution in pure water. 3: Twice re-crystallized DDAPS in 0.050 M NaF solution

screening from the charged electrolyte ions [24]. The similarity of the CMC values implies that this effect is not pronounced.

The data in Fig. 2 may be used to determine the Gibbs excess of DDAPS at the air-solution interface with the help of the Gibbs equation:

$$\Gamma = \frac{\partial \pi}{RT \partial \ln c_{\mathrm{DDAPS}}} \quad (1)$$

To apply Eq. 1, the surface pressure data below the CMC was fit to a polynomial (third order) function and the Gibbs excess of DDAPS adsorbed at the air-solution interface was calculated from the derivative of the polynomial. The Gibbs excesses determined by this procedure are plotted versus the logarithm of the bulk surfactant concentration in Fig. 3. The data show that at concentrations of DDAPS approaching the CMC, the surface concentration of DDAPS reaches a value $\sim 5.5\times10^{-10}$ mol cm^{-2} in the absence of NaF (filled black triangles) and is slightly lower ($\sim 5.2\times10^{-10}$ mol cm^{-2}) for the electrolyte-containing solution (open white triangles). This result is in excellent agreement with the value of $\Gamma = 5.5\times10^{-10}$ mol cm^{-2}reported in the literature [24].

Cyclic voltammetry

Cyclic voltammetry was used to qualitatively characterize the electrochemical behavior of DDAPS at the metal/solution interface. Figure 4 shows the CV curves of various DDAPS concentrations in 50 mM NaF supporting electrolyte recorded between −700 mV and 500 mV (versus Ag/AgCl), with a sweep rate of 20 mV s^{-1}. In this range, the Au(111) electrode is ideally polarized and the interface between the electrode and the solution has the property of a capacitor. More positive potentials were not investigated to avoid complications from OH^- adsorption [25]. A pair of peaks can be seen on the CV curve in the presence of the surfactant in the solution. These rather reversible peaks at approximately −500 mV correspond to the adsorption/desorption processes. These peaks are seen to progressively shift to more negative potentials with increasing surfactant concentration, indicating that DDAPS adsorption becomes thermodynamically favored as its concentration in the bulk of solution is raised. Another interesting feature of the cyclic voltammetry curves is the appearance of split adsorption peaks at [DDAPS]≥0.096 mM. Sotiropoluos [26] has previously cited the presence of split adsorption and desorption peaks in differential capacity measurements as evidence of the formation of surface micelles on mercury electrodes at bulk surfactant concentrations below the CMC.

Chronocoulometry

Chronocoulometry was used to quantitatively describe DDAPS adsorption at the Au(111) electrode surface. The charge density data determined by this technique were used for further thermodynamic analyses. The DDAPS concentrations studied in this work ranged from 0.032 mM to 10 mM, the latter being well above the CMC of DDAPS. In chronocoulometry, the Au(111)

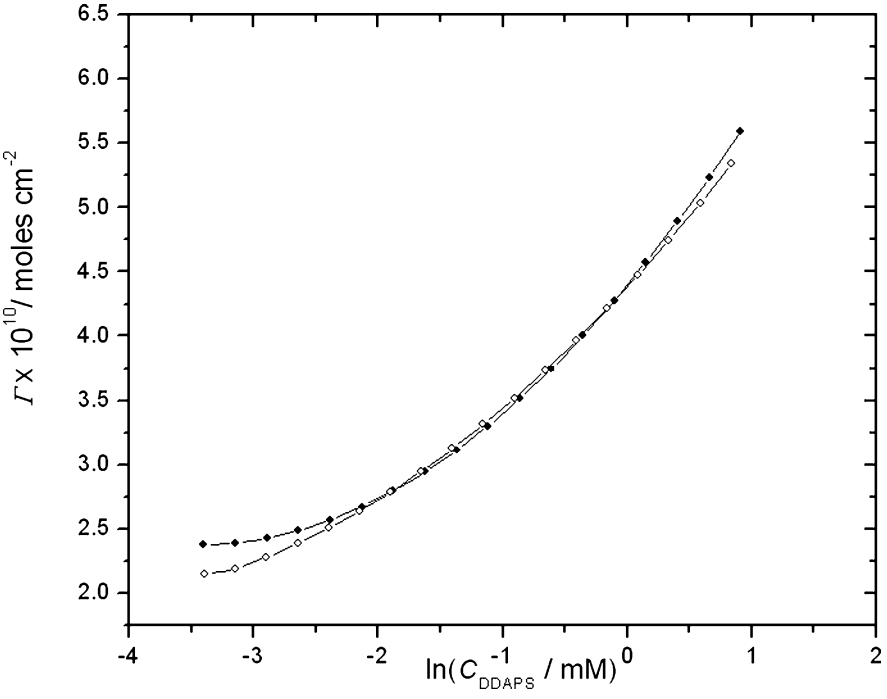

Fig. 3 The relative Gibbs excess of DDAPS at the air/solution interface plotted against the logarithm of the bulk DDAPS concentration at concentrations below the CMC. Filled points: pure water solution; unfilled points: 0.050 M NaF solution

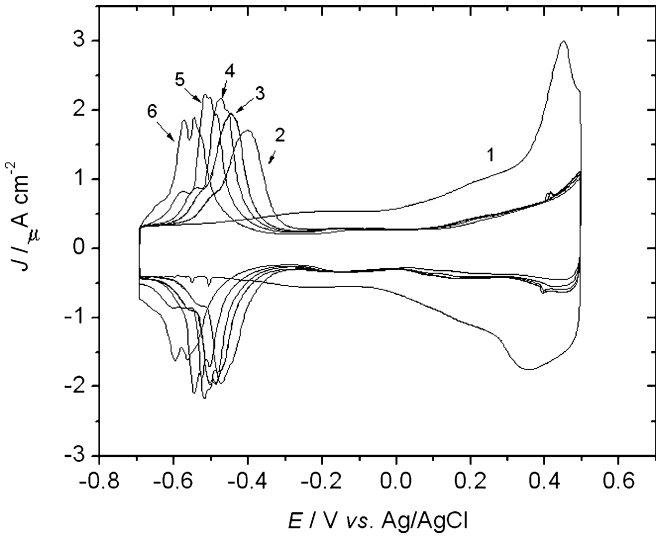

Fig. 4 Cyclic voltammetry curves recorded for the Au(111) electrode in 0.050 M NaF. 1: Without DDAPS; 2: [DDAPS] = 0.032 mM; 3: [DDAPS] = 0.064 mM; 4: [DDAPS] = 0.096 mM; 5: [DDAPS] = 0.160 mM; 6: [DDAPS] = 0.3 mM; sweep rate 20 mV/s

electrode was maintained at a selected potential E_{ads} for three minutes to establish the adsorption equilibrium. During this time, the solution was stirred to ensure the maximum rate of mass transport. The stirrer was turned off and the solution was allowed to settle before the potential was stepped to the desorption potential, $E_{des} = -1000$ mV. The current transient due to the desorption of the surfactant molecules and to the recharging of the double layer was measured and subsequently integrated to determine the difference between the charge density on the electrode surface at potentials E_{ads} and E_{des}. This procedure was repeated by varying the potential E_{ads}between −950 mV to 500 mV in 25 or 50 mV increments. From the position of the diffuse layer minimum in the differential capacity curve of the electrode in a 5 mM NaF solution, the potential of zero charge (pzc) was determined to be equal to 310 mV. The absolute charge at the electrode surface was then calculated from the measured difference of the charge densities and the pzc as described in [27, 28].

The charge density plots of various concentrations of DDAPS in 50 mM NaF supporting electrolyte are plotted as a function of potential in Fig. 5. Consistent with the results obtained from CV, the charge density curves for DDAPS and pure supporting electrolyte solutions merged at very negative potentials, indicating that DDAPS is not adsorbed at these potentials. The charge density curves exhibit three distinct regions as indicated by the Roman numerals in Fig. 5. In region I the curves initially coincide with the curve for the pure electrolyte but then exhibit a sigmoidal inflexion indicative of the adsorption of the surfactant. Region II is characterized by a linear rise in the charge density with increasingly positive potentials. Region III also exhibits a linear charge dependence on the applied electrode potential but the slope of the curve is larger than that of region II. At the positive limit of region III, the charge density increases rapidly as a function of E. As the pH of the supporting electrolyte is close to 9, hydroxide

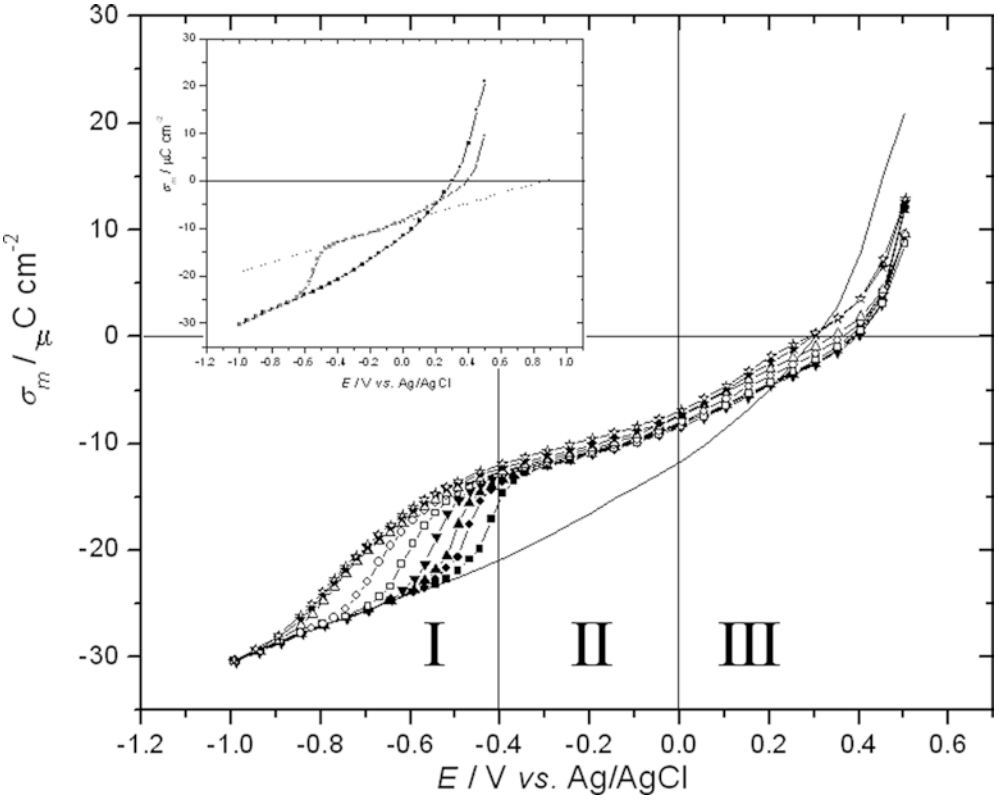

Fig. 5 Charge density versus electrode potential plots for the Au (111) electrode in contact with 0.050 M NaF solution, with the following DDAPS concentrations: solid line: 0; filled squares: 0.032; filled circles: 0.096; filled triangles: 0.160; filled upside-down triangles: 0.30; unfilled squares: 0.60; unfilled circles: 1.10; unfilled triangles: 2.20; filled stars: 3.0; unfilled stars: 10.0 mM. Inset: charge density plots for the pure supporting electrolyte and for 0.3 mM DDAPS solutions

adsorption and pre-oxidation of the gold surface starts in this range of applied potentials [25], making it impossible to separate these processes from any structural changes in the adsorbed DDAPS layer.

The charge density data provide information on the orientation of the surfactant molecules in regions II and III. The charge density curve shows that the potential of zero charge is shifted in the presence of DDAPS. The change in the potential of zero charge (ΔE_{pzc}) due to the displacement of surface water by a film of adsorbed molecules is described by [28, 29]:

$$\Delta E_{pzc} = \Gamma_{max}\left(\mu_{org} - n\mu_{w}\right)/\varepsilon \qquad (2)$$

in which Γ_{max} is the maximum surface concentration of the organic molecules, μ_{org} and μ_{w} are the average components of the permanent dipole moment in the direction normal to the surface of the organic molecule and water respectively, n is the number of water molecules displaced from the electrode surface by one adsorbed organic molecule, and ϵ is the permittivity of the inner layer. Determination of ΔE_{pzc} for region III is readily obtained from the intersection of the charge density plot with the zero line of the ordinate axis. E_{pzc} ranges from ~420 mV for the lowest concentration of DDAPS to ~310 mV for the highest DDAPS, meaning the value of ΔE_{pzc} changes from ~100 to ~0 mV with the bulk DDAPS concentration (the latter value is observed in solutions with DDAPS concentration higher than the CMC). Inspection of Eq. 2 reveals that the term in the brackets dictates the sign of ΔE_{pzc}. At the pzc, water molecules are known to be weakly preferentially oriented with the oxygen atom turned towards the Au(111) surface [30]. At the pzc of a polycrystalline gold electrode, Beccuci et al [31] estimated the surface potential of oriented water molecules to be −640 mV. The (111) surface of gold is more hydrophobic than the polycrystalline surface [32] and hence this number must be smaller. In order for ΔE_{pzc} to be small, μ_{org} must be small as well. Consequently, in region III, DDAPS molecules that replace the solvent on the electrode surface must be oriented such that their dipole moment forms a small angle with the interfacial plane with the negative pole of the dipole facing the metal.

To determine ΔE_{pzc} in region II, a line with a slope of 11 μF cm^{-2} is carried through the charge densities in region II and extrapolated to$\sigma_m = 0$, as shown in the inset to Fig. 5 for the example of the charge density curve for 0.3 mM DDAPS solution. Depending on the bulk concentration of DDAPS, E_{pzc} changes from approximately +900 mV (lowest concentration) to approximately +675 mV (highest concentration). Consequently, ΔE_{pzc} ranges from 580 mV to 355 mV and is a large positive value compared to the ΔE_{pzc} in region III. Such ΔE_{pzc} values indicate that in region II the DDAPS molecules must assume an orientation that gives a significant average dipole moment in the direction of the surface normal, with the positive pole of this dipole turned to the electrode and the negative pole toward the solution. Clearly a change in the electrode potential causes a significant reorientation of DDAPS molecules at the electrode surface.

To further analyze the behavior of DDAPS molecules in regions II and III, the differential capacities of the Au(111) electrode were calculated by numerical differentiation of the charge density curves. They are plotted in Fig. 6. These curves may be considered to be the zero frequency capacities representing the adsorption equilibrium. The inset to Fig. 6 compares the differential capacity calculated by the differentiation of the charge density curve to the capacity calculated from the CV and from the AC impedance measurements at a single frequency 25 Hz. The capacities calculated from the charge density curve agree well with the capacities determined from the cyclic voltammogram (although the split of the desorption peak is not seen on the $d\sigma_M/d\,E$ curve due to poorer resolution of the charge potential plot). This is not unexpected. The CV curves shown in Fig. 4 display quite symmetric adsorption desorption peaks characteristic of an equilibrium adsorption. In contrast, the curve determined from the single frequency AC impedance measurement displays much smaller pseudocapacity peaks, indicating that the adsorption/desoption and the film relaxation processes are too slow to follow the potential modulation at the frequency of 25 Hz.

The plots of $d\sigma_m/dE$ clearly demonstrate that the capacity curves have two minima within the potential region of DDAPS adsorption at the Au(111) electrode surface. In region II (−400 mVE < −100 mV) the capacity reaches a minimum of ~11 μF cm^{-2}. In contrast, the second minimum capacity in region III (200 mVE < 300 mV) is ~21 μF cm^{-2}, nearly double the capacity of region II. A broad and not well-pronounced peak at ~100 mV corresponds to the phase transition between the two states.

In conclusion, the analysis of the charge density data indicates that the adsorption of DDAPS has a two state character. Each of the two states is characterized by a different value for the pzc and a different minimum value for the capacity. Each state corresponds to a different orientation of DDAPS molecules at the gold electrode surface. The transition between these states is potential controlled.

Surface pressure and Gibbs excess

The surface pressure due to the adsorption of DDAPS on the Au(111)-solution interface was calculated by integrating the charge density versus electrode potential plot obtained from the chronocoulometry experiments as described in Eq. 3:

$$\pi = \gamma_0 - \gamma = \left(\int_{E_{des}}^{E} \sigma_m dE\right)_{[DDAPS]} - \left(\int_{E_{des}}^{E} \sigma_m dE\right)_{[DDAPS]=0} \qquad (3)$$

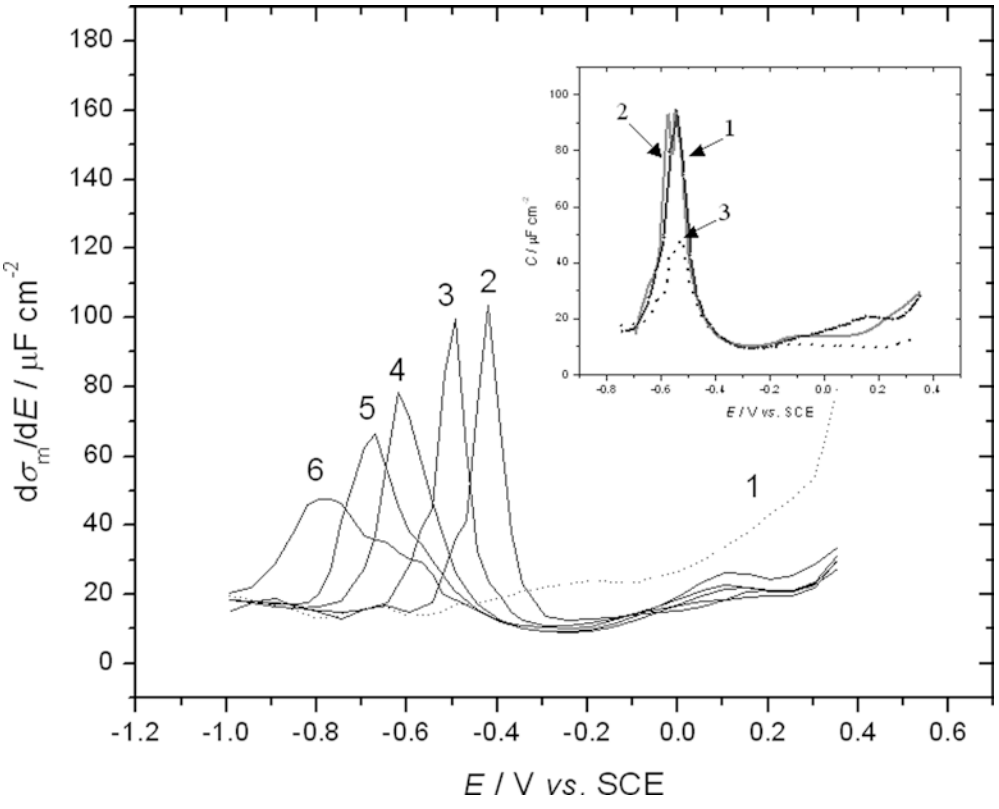

Fig. 6 Differential capacity curves calculated by differentiation of the charge density plots for the Au(111) electrode in contact with 0.050 M NaF solution. Curve 1 and the dashed line are pure supporting electrolyte; solid lines have supporting electrolyte with the following concentrations of DDAPS: 2: 0.032 mM; 3: 0.160 mM; 4: 0.6 mM; 5: 1.1 mM; 6: 3.0 mM. Inset: for 0.3 mM DDAPS solution, comparison of the differential capacity curves calculated by: (curve 1) differentiation of the charge density plots; (curve 2) from the cyclic voltammetry curve recorded at 20 mV/s sweep rate; (curve 3) from AC impedance measurements using a 25 Hz, 5 mV rms AC perturbation and 5 mV s^{-1} potential sweep rate

where γ_o and γ represent the surface energy of the surfactant free and the surfactant covered electrode, respectively. The surface pressure is a measure of the energetics of DDAPS adsorption. Figure 7 plots the surface pressure π versus the electrode potential for several bulk DDAPS concentrations. The surface pressure data are seen to take the form of bell-shaped curves, and the maximum of the curve defines the potential of maximum adsorption, E_m, plotted as a function of the logarithm of DDAPS concentration in the inset to Fig. 7. These potentials correspond to the intersection points of the charge density curve for a DDAPS solution with the charge density curve for the pure electrolyte. For all DDAPS concentrations, the value of E_m is seen to be confined to exist within region III. At low concentrations of DDAPS, the potential of maximum adsorption is very weakly dependent on the surfactant concentration. However, as the concentration of DDAPS in the electrolyte is increased above 0.42 mM, the value of E_m is seen to move progressively toward more positive potentials.

The potential of maximum adsorption is related to ΔE_{pzc} by the following equation [29, 33]:

$$\left(E_m - E_{pzc}\right) = -C_{\theta=1}\Delta E_{pzc}/(C_0 - C_{\theta=1}) \quad (4)$$

where $C_{\theta=1}$and C_0 are the capacities of the gold electrode fully covered and DDAPS free respectively. Consistent with Eq. 4 and the earlier discussion of ΔE_{pzc}, the E_m values are negative with respect to E_{pzc} at low DDAPS concentrations (where ΔE_{pzc} is positive) and are equal to zero for 3 and 10 mM solutions of DDAPS (above the CMC) where ΔE_{pzc} is equal to zero as well. Therefore, the dependence of E_m on the DDAPS concentration is caused by reorganization of the adsorbed DDAPS molecules, which was discussed earlier.

The Parsons' function $\xi = \sigma_M E + \gamma$ [34] has been calculated independently from the experimental data, and the film pressure at a constant charge $\Phi = \zeta_0 - \zeta_\theta$ [35] has been determined. The calculated values of Φ are plotted against the charge density in Fig. 8.

For DDAPS concentrations higher than 0.4 mM, the shape of the Φ versus σ_M plots can be seen as being composed of two overlapping bell shape curves with maxima at negative charge densities and close to zero charge, respectively. Clearly, the analysis based on charge as the independent electrical variable also shows that DDAPS adsorption at the Au(111) electrode surface has a two state character.

By differentiating the surface pressure versus natural logarithm of the bulk DDAPS concentration at constant E, the relative Gibbs surface excess Γ can be determined:

$$\Gamma = \left(\frac{\partial \pi}{RT\partial \ln c_{DDAPS}}\right)_E \quad (5)$$

As the activity of DDAPS is nearly constant above the CMC, the differentiation is limited to DDAPS concentrations below the bulk solution's critical micelle concentration. The results of the differentiation are illustrated in Fig. 9A, where Γ is plotted as a function

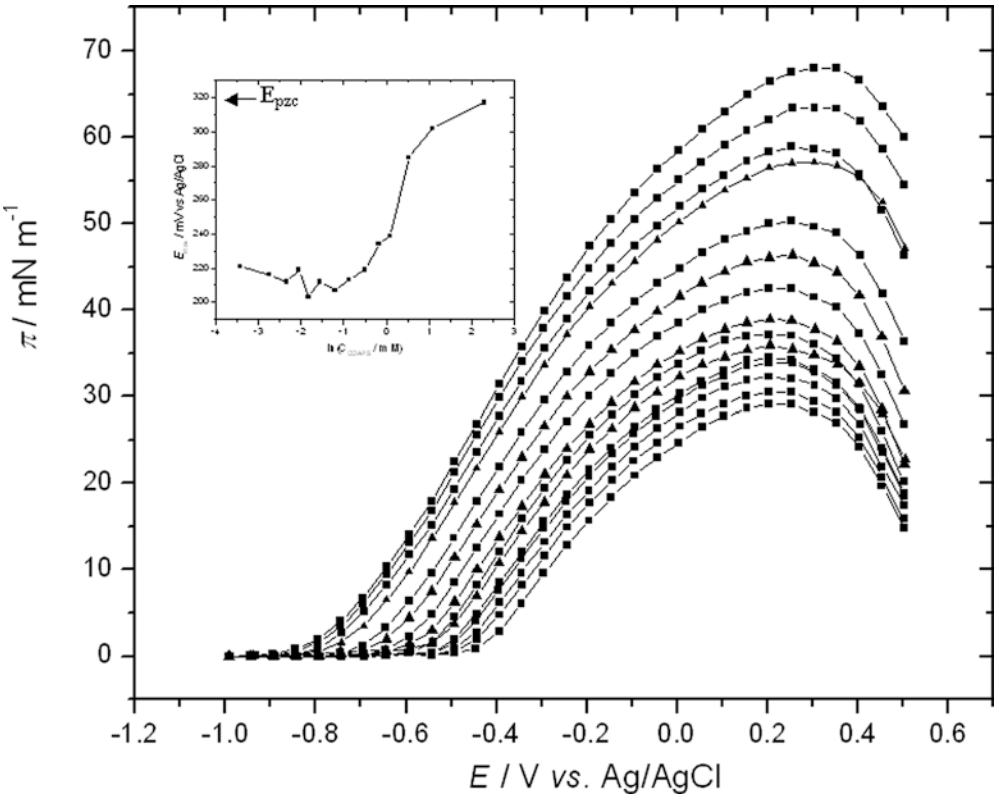

Fig. 7 Plots of the surface pressure of DDAPS at the gold-solution interface versus the electrode potential for various bulk DDAPS concentrations equal to (curves from the bottom to the top): 0.032; 0.064; 0.096; 0.128; 0.160; 0.21; 0.30; 0.42; 0.60; 0.84; 1.10; 1.68; 2.20; 3.0; 10.0 mM. Inset: plot of the potential of the maximum adsorption versus the logarithm of the bulk DDAPS concentration

of the electrode potential for the DDAPS concentrations studied. At very low DDAPS concentrations, the Gibbs excess is higher in region II then it is in region III. Qualitatively this agrees with the differential capacity values obtained from differentiation of the charge density curves in Fig. 7 which show a significantly higher capacity for region III compared to region II.

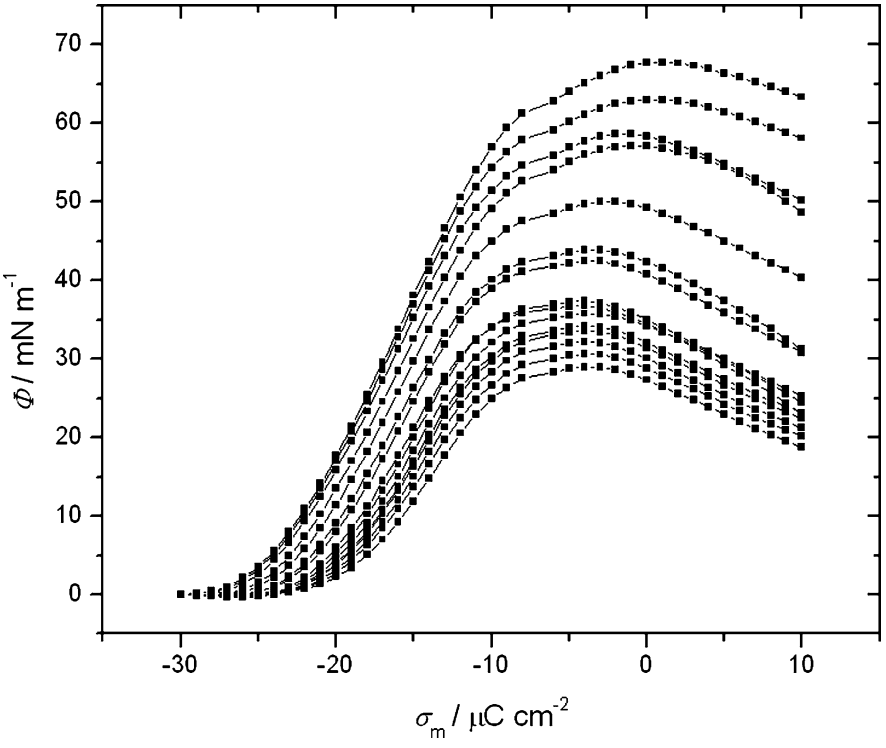

Fig. 8 Plots of the surface pressure of DDAPS at the gold-solution interface versus charge density at the metal surface for various bulk DDAPS concentrations equal to (curves from the bottom to the top): 0.032; 0.064; 0.096; 0.128; 0.160; 0.21; 0.30; 0.42; 0.60; 0.84; 1.10; 0.1.68; 2.20; 3.0; 10.0 mM

However, in solutions with DDAPS concentration lower than 0.3 mM, the Gibbs excess attains the maximum value in region II while the maximum of the film pressure is observed in region III. This difference may be explained assuming that the DDAPS adsorption is described by the generalized Frumkin isotherm [35]. In that case, the film pressure of adsorbed DDAPS is described by the equation [36]:

$$\pi = RT\Gamma[\ln(c) + \ln n_w\beta + n_w a - (n_w - 1)] \quad (6)$$

where a is the so called lateral interaction constant and β is the equilibrium constant related to the zero coverage Gibbs energy of adsorption by the formula $\Delta G^0_{ads} = -RT\ln\beta$. Equation 6 shows that the maximum of the $\pi(E)$ plot may not coincide with the maximum of the $\Gamma(E)$ curve if the adsorbed molecules reorient with potential such that they occupy a larger area per molecule at the surface in region III but give a much more negative value of ΔG_0 and hence a much higher value of β. By moving with potential from region II to region III, the increase in the "ln $n_w\beta$" term must be significant to compensate for the decrease of the Gibbs excess.

At higher DDAPS bulk concentrations, the dependence of the Gibbs excess on the electrode potential is more complicated. These curves are characterized by a plateau in the $\Gamma(E)$ plot for potentials corresponding to region II followed by an ascending Gibbs excess as the potential is increased into the domain of region III. The width of potentials spanned by the plateau (region II) is seen to systematically shrink with increasing DDAPS concentration. The maximum Gibbs excess in the region of the plateau is 4.0×10^{-10} mol cm^{-2}. For higher DDAPS concentrations, the Gibbs excess is twice as high as the Gibbs excess at the plateau with increasing positive potential. These much higher Gibbs excesses indicate that there may be a transition from two-dimensional to three-dimensional adsorption in region III as the surfactant concentration is increased. The underlying, horizontal DDAPS molecules would serve as the foundation for three-dimensionally aggregating structures as previously visualized using STM and AFM imaging for SDS [21, 22]. Such changes in the surface composition can be described with the help of the theory developed by Retter et al [17, 18, 19, 20]. We are presently acquiring STM and AFM images of the various states of the film and will discuss their structure more quantitatively in the next publication.

Independently, the Gibbs excess at constant charge was calculated by plotting the Parsons' function $\xi = \sigma_M E + \gamma$ [34] and differentiating the relative ξ versus the logarithm of the bulk DDAPS concentration. The relative Gibbs excesses are plotted as a function of the electrode charge density in Fig. 9B. For the intermediate bulk DDAPS concentrations, the Gibbs excess plots display two maxima, one at charge densities of approximately -10 μC cm^{-2} and the second at ~3 μC cm^{-2}. The results also show that when charge is used as the independent electrical variable, the transition from region II to region III is gradual.

Gibbs energy of adsorption and charge numbers per adsorbed molecule

The standard Gibbs energy of adsorption, ΔG^o_{ads}at zero coverage, has been determined from the initial slopes of the surface pressure π versus mole fraction of DDAPS plot using the Henry's Law isotherm [25]:

$$\pi = RT\Gamma\beta\frac{c}{55.5} \quad (7)$$

where $\beta = \exp\left(\frac{-\Delta G^0_{ads}}{RT}\right)$. The standard state was defined as being the unit mole fraction of DDAPS in the bulk and a monolayer coverage of non-interacting DDAPS molecules at the surface. The Henry isotherm could only be applied to describe DDAPS adsorption at the most negative potentials corresponding to region II. Therefore, in the calculation of ΔG^0_{ads}, the maximum surface coverage 4.0×10^{-10} mol cm^{-2} was used for Γ_{max}. The ΔG^0_{ads}values are plotted against the electrode potential in Fig. 10A.

Similarly, the film pressures at constant charge and Eq. 7 were used to calculate the zero coverage Gibbs energies of adsorption for charge as the independent electrical variable. These values of $\Delta G^0_{ads}$are plotted against the charge densities in Fig. 10B. The Gibbs energies at constant potential and constant charge vary from approximately -10 to -33 kJ mol^{-1}. These values are characteristic of physical adsorption of an organic molecule at a gold surface [28], and suggest that in region II the interactions between the adsorbed molecule and the gold surface are weak. Interestingly, comparable magnitudes for the Gibbs energies of adsorption were observed for SDS adsorption at the gold electrode surface [22].

Conclusions

Chronocoulometric experiments provided charge density data that allowed us to describe the thermodynamics of DDAPS aggregation on the Au(111) electrode surface. We have used charge densities to determine the surface pressure of the film-covered electrode surface, Gibbs excesses, and the zero coverage energies of adsorption. The main results of this work are summarized in Fig. 11 which shows the Gibbs excess data in a three-dimensional representation with the electrode potential and the bulk surfactant concentration as variables on the basal plane. The various states of DDAPS adsorption are indicated on the surface of the grid.

Our results indicate that molecules start to adsorb onto the electrode surface at potentials between -600 mV and -400 mV, depending on the bulk concentration of DDAPS. The DDAPS molecules

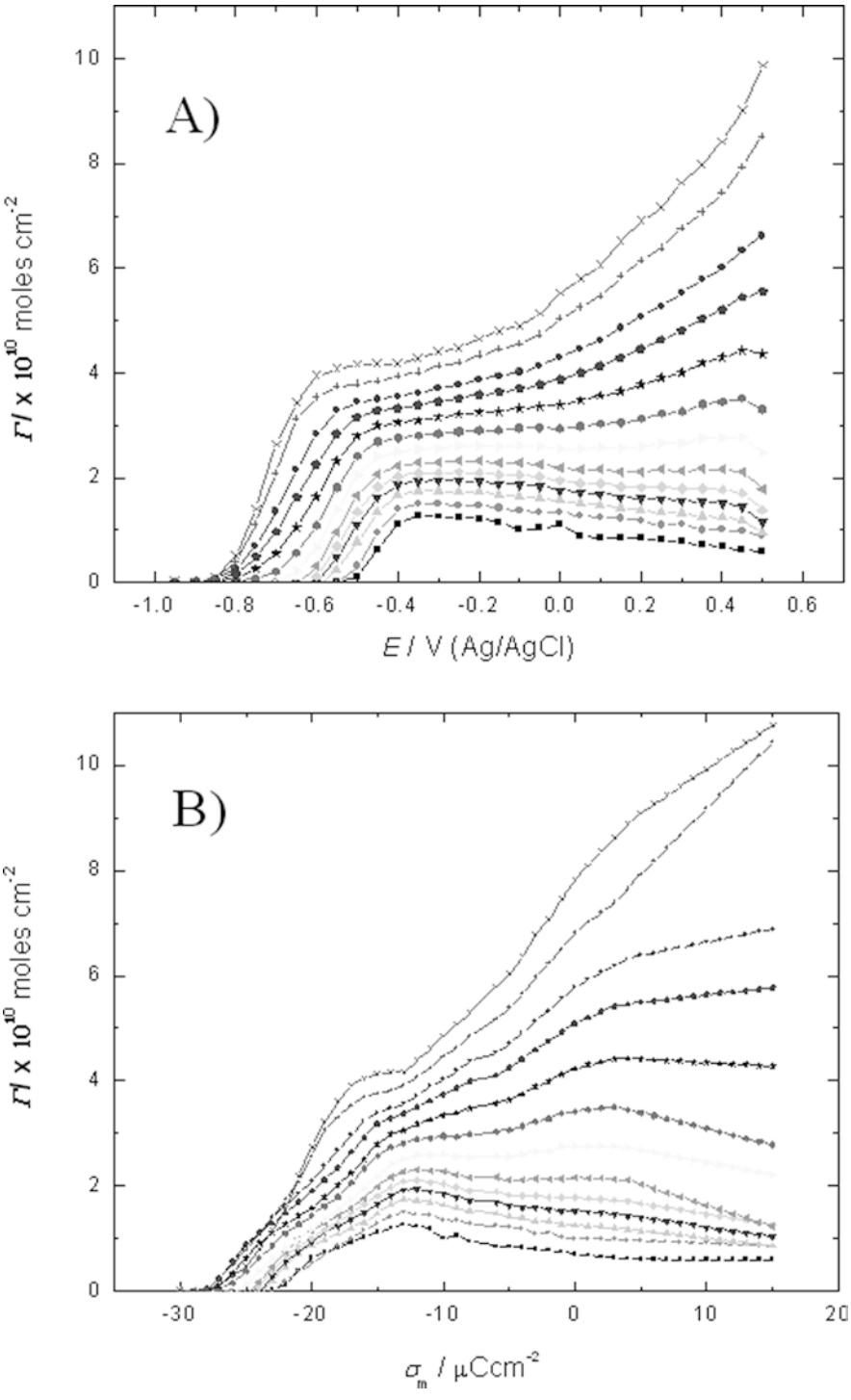

Fig. 9 A Plot of the Gibbs excess of DDAPS versus the electrode potential for various bulk DDAPS concentrations; curves (from the bottom to the top) correspond to: 0.032; 0.096; 0.160; 0.30; 0.60; 1.10; 2.20; 3.0; 10.0 mM. B: Plot of the Gibbs excess of DDAPS versus charge density at the metal surface for various bulk DDAPS concentrations; curves (from the bottom to the top) correspond to: 0.032; 0.096; 0.160; 0.30; 0.60; 1.10; 2.20; 3.0; 10.0 mM

exhibit two discrete states of adsorption. In the region of potentials between approximately -600 mVE < -100 mV, the surfactant molecules assume a tilted orientation in which the hydrocarbon tails are directed towards the metal and the polar head towards the solution. The zero coverage Gibbs energies of adsorption determined in this region are higher than -33 kJ mol^{-1} and are hence characteristic of a physisorbed state.

At more positive electrode potentials $\sim$100 mVE $< \sim$300 mV, the structure of the film depends strongly on the bulk DDAPS concentration. When the surfactant concentration is low, the molecules are oriented almost horizontally to the electrode surface. At higher concentrations of DDAPS in the bulk electrolyte, the Gibbs excess is much higher than the value expected for a horizontal orientation. We propose a three-dimensional aggregation, or micellization, to

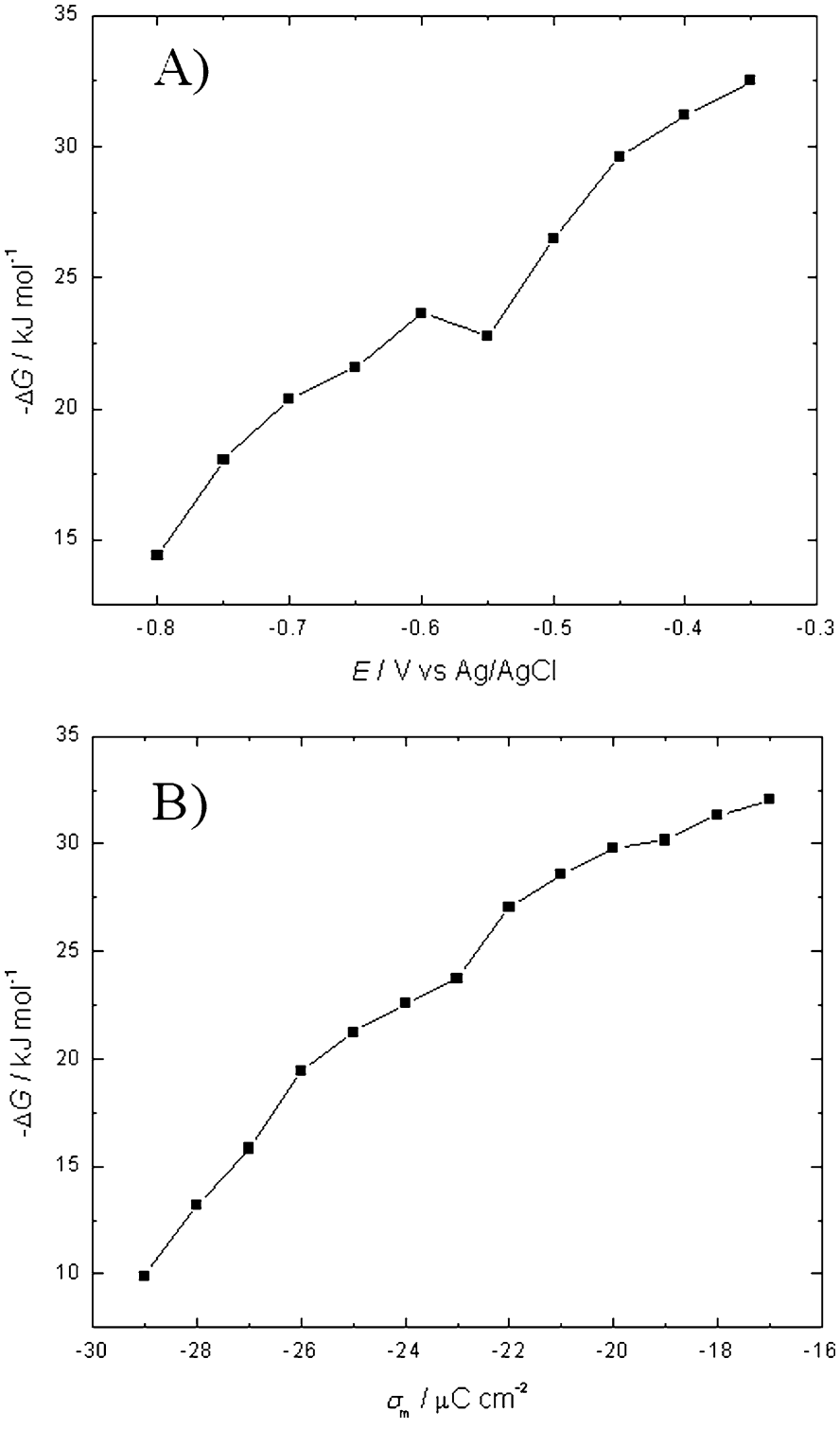

Fig. 10 The zero coverage Gibbs energies of adsorption plotted as a function of the electrode potential **A** and charge density **B**

explain this result. With only data from the electrochemical experiments it is impossible to determine the exact geometry of the aggregate, but the small shift in E_{pzc} implies that the average permanent dipole moment of the adsorbed molecules must be nearly parallel to the electrode surface. Possible geometrical aggregates that satisfy this observation include full cylinders, as observed by Ducker and Wanless for DDAPS adsorption on pyrolitic graphite, and hemi-cylindrical aggregates with the individual surfactant molecules aligned co-linear with the long-axis of the cylinder.

In our next paper on DDAPS adsorption we will provide the results of STM imaging in an effort to fully characterize the field-driven and concentration-

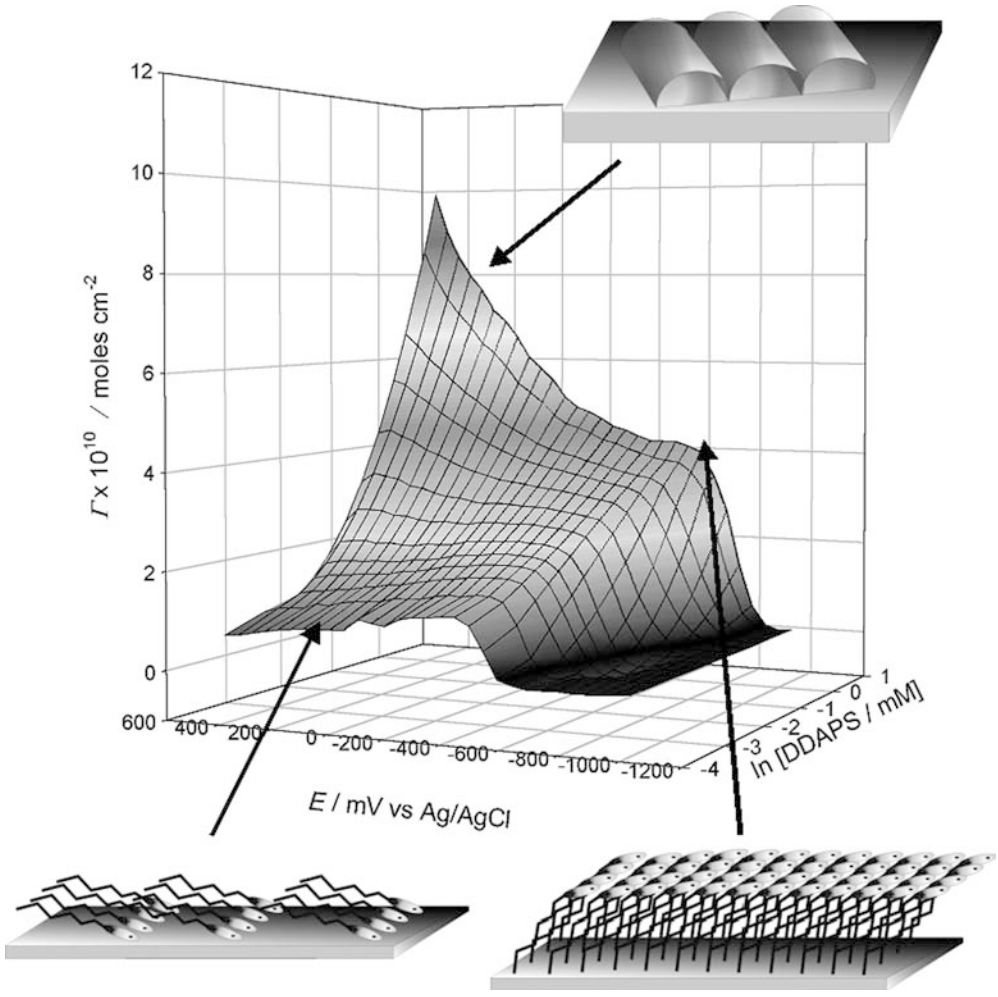

Fig. 11 Gibbs excess plots and schematic representation of the change in the orientation of DDAPS molecules as a function of the electrode potential in solutions of the lowest DDAPS concentration (0.032mM) and at the CMC of DDAPS (2.2mM)

dependent changes in the adsorption of this zwitterionic surfactant. It is expected that this work will clarify the issue of the nature of the aggregate geometry.

Acknowledgements We would like to thank Professor Dan Bizzotto (University of British Columbia) for supplying us with the software used to collect the electrochemical data. This work has been supported by a grant from the Natural Sciences and Engineering Research Council of Canada. JL acknowledges the Canada Foundation for Innovation for the Canada Research Chair Award.

References

1. Manne S, Cleveland JP, Gaub HE, Stucky GD, Hansma PK (1994) Langmuir 10:4409
2. Manne S, Gaub HE (1995) Science 270:1480
3. Manne S (1997) Prog Coll Pol Sci 103:226
4. Jaschke M, Butt H-J, Gaub HE, Manne S (1997) Langmuir 13:1381
5. Wolgemuth JL, Workman RK, Manne S (2000) Langmuir 16:3077
6. Wanless E J, Ducker WA (1996) J Phys Chem 100:3207
7. Wanless EJ, Davey TM, Ducker WA (1997) Langmuir 13:4223
8. Liu J-F, Ducker WA (2000) Langmuir 16:3467
9. Liu J-F, Min G, Ducker WA (2001) Langmuir 17:4895
10. Subramanian V, Ducker WA (2000) Langmuir 16:4447
11. Schulz JC, Warr GG, Butler P, Hamilton WA (2001) Phys Rev E 63:041604
12. Wanless EJ, Ducker WA (1997) Langmuir 13:1463
13. Ducker WA, Wanless EJ (1996) Langmuir 12:5915
14. Ducker WA, Grant LM (1996) J Phys Chem 100:11507
15. Grant LM, Ducker WA (1997) J Phys Chem B 101:5337
16. Grant LM, Tiberg F, Ducker WA (1998) J Phys Chem B 102:4288
17. Retter U (2000) Langmuir 16:7752
18. Retter U, Avranas A (2001)Langmuir 17:5039
19. Retter U, Tchachnikova M, Avranas A (2002) J Colloid Interf Sci 251:94
20. Retter U, Tchachnikova M (2003) J Electroanal Chem 550–551:201
21. Burgess I, Jeffrey CA, Cai X, Szymanski G, Galus Z, Lipkowski J (1999) Langmuir 15:2607
22. Burgess I, Zamlynny V, Szymanski G, Lipkowski J, Majewski J, Smith G, Satija S, Ivkov R (2001) Langmuir 17:3355
23. Petri M, Kolb DM (2002) Phys Chem Chem Phys 4:1211
24. Weers JG, Rathman JF, Axe FU, Crichlow CA, Foland LD, Scheuing DR, Wiersema RJ, Zielske AG (1991) Langmuir 7:854.
25. Chen A, Lipkowski J (1999) J Phys Chem 103:682
26. Sotiropoulos S, Nikitas P, Papadopoulos N (1993) J Electroanal Chem 356:201
27. Richer J, Lipkowski J (1986) J Electrochem Soc 133:121
28. Lipkowski J, Stolberg L (1992) In: Lipkowski J, Ross PN (eds) Adsorption of molecules at metal electrodes. Wiley-VCH, New York, pp171
29. Trasatti S (1974) J Electroanal Chem 53:335

30. Ataka K, Yotsuyanagi T, Osawa M (1996) J Phys Chem 100:10664
31. Becucci L, Moncelli MR, Guidelli R (2003) Langmuir 19:3386
32. Lipkowski J, Nguyen Van Huong C, Hinnen C, Parsons R, Chevalet J (1983) J Electroanal Chem 143:375
33. Parsons R (1961) Proc R Soc Lon Ser–A 261:79
34. Parsons R, Trasatti S (1986) J Electroanal Chem 205:359
35. Damaskin BB, Petrii OA, Batrakov VV (1968) Adsorption of organic compounds on electrodes. Nauka, Moscow
36. Yang DF, Stolberg L, Lipkowski J, Irish DE (1992) J Electroanal Chem 329:259